Smart Materials and Structures

PAPER • **OPEN ACCESS**

Effects of membrane surface pretreatment on ionic polymer-metal composite (IPMC) actuation and scanning electrochemical microscopy (SECM) analysis

To cite this article: Jung Hwa Lee *et al* 2025 *Smart Mater. Struct.* **34** 095018

OPEN ACCESS
IOP Publishing
Smart Materials and Structures
Smart Mater. Struct. **34** (2025) 095018 (10pp)
https://doi.org/10.1088/1361-665X/ae02cf

Effects of membrane surface pretreatment on ionic polymer-metal composite (IPMC) actuation and scanning electrochemical microscopy (SECM) analysis

Jung Hwa Lee[1], **Jongcheol Lee**[1], **John Albert Faccinto** and **Kwang J Kim***

Active Materials and Smart Living (AMSL) Laboratory Department of Mechanical Engineering, University of Nevada-Las Vegas (UNLV) 4505 S Maryland Pkwy, Las Vegas, NV 89154, United States of America

E-mail: kwang.kim@unlv.edu

Received 28 May 2025, revised 23 July 2025
Accepted for publication 3 September 2025
Published 11 September 2025

Abstract

This study investigates how membrane surface pretreatment, including sanding and chemical cleaning, affects the electrochemical and mechanical performance of ionic polymer–metal composites. IPMC samples fabricated under varying surface pretreatment conditions were characterized in terms of electrode morphology, surface resistance, water uptake, electrode thickness, and actuation behavior. Scanning electrochemical microscopy (SECM) was employed to visualize cross-sectional electrode architecture and assess local electrochemical activity. Results show that surface roughening promotes thicker, more continuous platinum electrode layers with deeper membrane penetration, reduced surface resistance, and more stable and amplified actuation. While cleaning alone decreased water uptake, it enhanced surface conductivity and actuation compared to uncleaned samples. The fully treated IPMC, which combined sanding and cleaning, exhibited the largest and most stable tip displacement. SECM imaging provided direct spatial mapping of electrochemically active regions, distinguishing the electrode and membrane domains. These findings underscore the critical role of membrane surface pretreatment in optimizing IPMC performance and highlight the potential of SECM for advancing the fundamental understanding and design of high-efficiency ionic soft actuators.

[1] J H Lee and J Lee contributed equally to this work.
* Author to whom any correspondence should be addressed.

Supplementary material for this article is available online

Keywords: ionic polymer–metal composite (IPMC), membrane surface pretreatment, scanning electrochemical microscopy (SECM)

1. Introduction

Ionic polymer–metal composites (IPMCs) are promising transducers that operate effectively in aqueous environments and have been actively studied for applications in diverse fields including bioinspired underwater robotics [1–4], medical devices [5, 6], wearable electronics [4, 7–9], and energy harvesting [10, 11]. An IPMC possesses a sandwich-like structure, consisting of an ionic polymer membrane positioned between two conductive electrode layers. The membrane interlayer facilitates ion transport, while the electrodes serve as electron conductors [10, 12]. The migration of hydrated cations under an applied electric field induces asymmetric swelling across the membrane thickness, resulting in bending of the IPMC toward the anode [12]. As this electromechanical behavior is closely linked to the morphology and continuity of the electrode–membrane interface, fabrication processes that control surface structure and material deposition are critical to device performance.

There have been efforts to improve IPMC actuation and sensing performance through optimization of fabrication parameters [4, 13–17]. Kim and Shahinpoor reported an inverse relationship between electrode surface resistance and the maximum blocking force of IPMCs, and demonstrated that additional electroplating with silver or copper enhanced actuation performance by improving surface conductivity [18]. Chang *et al* systematically investigated the effects of membrane roughening (e.g. sandpaper grit) and the number of impregnation-reduction and autocatalytic plating cycles on electrode morphology and mechanical behavior [13]. They found that while increased plating cycles reduced sheet resistance and enhanced electrode thickness and penetration, roughened membranes led to lower elastic modulus and more compliant electrode layers—favorable for actuation. Wang *et al* further emphasized that the combination of surface roughening and optimized plating steps significantly influenced physical parameters such as surface resistance, electrode penetration depth, and dielectric modulus [14, 17]. These physical factors were found to jointly determine the deformation behavior of IPMCs, as samples with low surface resistance, low bending stiffness, and well-penetrated electrodes exhibited the most favorable electromechanical response. However, the individual and combined effects of membrane surface pretreatment steps—specifically sanding and chemical cleaning—on electrode structure, interfacial properties, and overall IPMC actuation performance remain insufficiently characterized. Although ion type and hydration state can influence IPMC behavior [17, 19, 20], these parameters were held constant in the present study to isolate the effects of surface pretreatment.

In electrochemical characterization of IPMCs, various techniques have been employed, including surface resistance measurement, cyclic voltammetry (CV), and impedance spectroscopy. Among these, surface resistance reflects the continuity of the electrode layer, and lower resistance is often associated with improved IPMC actuation performance, possibly due to a more uniform distribution of electric potential [14]. However, surface resistance can vary depending on the electrode structure and the quality of contact between the electrode and measurement probes, especially for rough IPMC surfaces. These variations make surface resistance an indirect and sometimes inconsistent indicator of IPMC performance. Cyclic voltammetry and electrochemical impedance spectroscopy provide information on the bulk electrochemical performance and overall capacitive behavior of IPMCs [7, 12, 21–23], but the local electrochemical information at the micrometer scale is limited.

Scanning electrochemical microscopy (SECM) offers a complementary approach for probing local electrochemical behavior of IPMCs. SECM can map the microtopography and spatially resolved electrochemical activity of surfaces in the presence of a redox mediator and supporting electrolyte solution using ultramicroelectrodes (UMEs) [24, 25]. When a potential that is sufficient to oxidize or reduce the redox species is applied to the UME probe, a steady state, diffusion-controlled current flows. This current varies depending on the electrochemical properties of the surface beneath the probe and the tip-surface distance, providing localized information about the sample surface. Compared to other electrochemical scanning probe microscopy techniques such as electrochemical scanning tunneling microscopy and conductive atomic force microscopy, SECM offers the advantage of non-contact measurements of redox activity and the ability to operate in liquid environments without requiring mechanical contact or electrical continuity with the sample [26]. Thus, SECM provides a useful combination of electrochemical sensitivity, micrometer-scale spatial resolution, and compatibility with hydrated, soft materials, making it suited for IPMC characterization.

In this study, we investigate the effects of membrane surface pretreatment, specifically sanding and chemical cleaning using hydrogen peroxide and acid, on the electromechanical performance and electrochemical properties of IPMCs. IPMC samples fabricated under different pretreatment conditions were systematically characterized in terms of electrode surface morphology, surface resistance, electrode thickness, water uptake, and actuation performance. Also, SECM was employed to visualize the spatial distribution of local electrochemical activity across the

cross-sections of the IPMCs. Our results demonstrate that membrane surface pretreatment significantly alters the structure and continuity of the electrode layers, which in turn governs ionic conductivity, redox activity and actuation stability. This work highlights the critical role of surface conditioning in optimizing IPMC fabrication and demonstrates the SECM analysis of IPMCs to resolve electrochemical features that are otherwise inaccessible through conventional measurements.

2. Materials and methods

2.1. IPMC fabrication

IPMCs with different membrane surface pretreatments were fabricated using the impregnation-reduction method (1st plating), followed by a surface electroding step (2nd plating) [27],as shown in figure 1. Tetraamineplatinum (II) chloride hydrate and Nafion^{TM} 117 (thickness of 183 μm, DuPont) were used for platinum electrode precursor and ionic polymer membrane, respectively.

Briefly, polymer membranes were sanded using #600 grit sandpaper and rinsed with DI water before sequential cleaning with hydrogen peroxide (H_2O_2) and sulfuric acid (H_2SO_4). To examine the effects of different membrane surface pretreatments, membranes underwent one, both, or neither of these procedures (see table 1). The pretreated samples were then immersed overnight in the platinum precursor solution to facilitate the adsorption of platinum complex ion, followed by reduction with sodium borohydride ($NaBH_4$). After this primary plating step, a secondary plating step was conducted using hydroxylamine hydrochloride and hydrazine as reducing agents in the platinum precursor solution. The fabricated samples were subsequently immersed in 1 M LiCl solution overnight for ion exchange prior to actuation testing. The specific fabrication conditions for each sample are summarized in table 1. For simplicity, IPMCs without pretreatment, with sanding only, with acid and peroxide cleaning only, and with both sanding and cleaning are referred to as non-pretreated (NP), sanding only (SD), cleaning only (CL), and fully treated (FT), respectively.

2.2. Physical and electromechanical characterization

The surface and cross-sectional morphologies of the IPMC films were imaged using a Hitachi TM3030 scanning electron microscopy (SEM) operated at 15 keV. Surface resistance measurements of the IPMC samples were measured under dry conditions using a multimeter with a 1 cm probe separation.

For the elongation rate, thickness swelling, and water content measurement, IPMC films fabricated with different surface treatments were cut into strips approximately 10 mm in length and 3 mm in width, ion-exchanged in 1 M LiCl, and then dried overnight. The length, thickness, and weight of these IPMC strips were measured both before and after hydration for five minutes in deionized water. The elongation rate, swelling, and water content were calculated using the equations below, and the results are summarized in table 2.

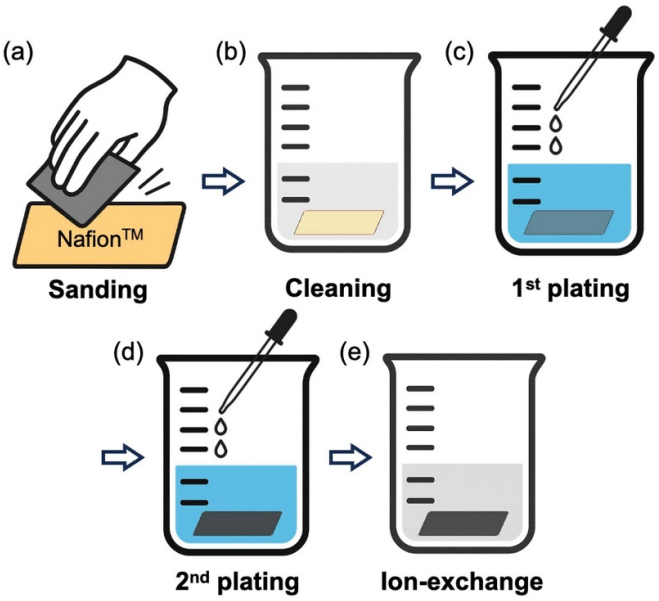

Figure 1. Fabrication steps for ionic polymer–metal composite (IPMC) films used in this study. The process includes: (a) membrane surface sanding, (b) acid/peroxide cleaning, (c) metal ion adsorption and reduction (primary plating or 1st plating), (d) surface electroding (secondary plating or 2nd plating), and (e) ion exchange in LiCl solution.

Table 1. Summary of IPMC samples fabricated with different membrane surface pretreatment combinations.

	Sanding	Cleaning
No pretreatment (NP)	X	X
Sanding only (SD)	O	X
Cleaning only (CL)	X	O
Fully treated (FT; sanding and cleaning)	O	O

$$\text{Elongation rate } (\%) = \frac{\text{length}_{\text{wet}} - \text{length}_{\text{dry}}}{\text{length}_{\text{dry}}} \times 100 \quad (1)$$

$$\text{Swelling } (\%) = \frac{\text{thickness}_{\text{wet}} - \text{thickness}_{\text{dry}}}{\text{thickness}_{\text{dry}}} \times 100 \quad (2)$$

$$\text{Water content } (\%) = \frac{\text{weight}_{\text{wet}} - \text{weight}_{\text{dry}}}{\text{weight}_{\text{dry}}} \times 100 \quad (3)$$

For actuation performance tests, IPMC strips were cut into 20 mm $\times$ 5 mm, ion-exchanged in 1 M LiCl, immersed in DI water, and subjected to an AC voltage of $\pm$1 V at 500 mHz. Tip displacement was recorded using a laser displacement sensor (optoNCDT-1401, Micro-Epsilon).

2.3. Electrochemical characterization

The surfaces and cross-sections of the IPMCs were analyzed using a (SECM; M370, BioLogic) in feedback mode. Platinum disk UMEs with diameters of 25 μm and 10 μm (SMP2045, Uniscan Instruments) were used as the working electrodes. A screen-printed Ag/AgCl electrode and a platinum sheet were used as the reference and counter electrodes, respectively. A solution containing 1 mM KI (redox mediator) and 100 mM NaCl (supporting electrolyte) was used. Constant-height SECM mapping was performed by scanning the UME tip across the *x*–*y* plane and simultaneously recording the tip current at room temperature in open air, without active humidity or evaporation control. A flat model sample with a 5 mm diameter gold disc (U-SECM-SAMPLE, BioLogic) was used as a reference. IPMC samples were embedded in either epoxy or UV-curable resin, cured, and then mounted for SECM analysis. Cross-sectional surfaces of the IPMCs were prepared by either cutting the resin-embedded samples with a razor blade or polishing them using 1000 nm colloidal alumina (1 wt%) on fiber cloth.

3. Results and discussions

3.1. Morphology of IPMC surface electrode

The surface morphology of IPMC electrodes exhibited variations that correlated with the membrane surface pretreatments, as shown in figure 2. While the Nafion™ membrane displays a flat and smooth surface (figure 2(a)), the IPMC samples (figures 2(b)–(e)) show rougher surfaces. Despite undergoing a secondary plating step, which is generally known to fill valleys and smoothen the roughness from the primary plating [14],noticeable morphological differences persist among the IPMC samples with different pretreatments. This difference is likely attributable to the formation of a thin surface electrode layer during the secondary plating. While the electrode thickness could not be determined from the cross-sectional SEM images (figure S1) due to sample tilting and imprecise cutting, the vertically sectioned samples embedded in UV resin (figure S2) showed that the electrode thicknesses are approximately 1–2.5 μm. Such a thin layer may be insufficient to mask the underlying morphology established during the primary plating, thus preserving the initial surface morphology.

Among the IPMCs with different pretreatments, the samples without sanding (NP and CL, figures 2(b) and (d)) exhibited wrinkle-like patterns interspersed with smooth surface domains approximately 15 μm in size. The presence of these smooth regions is consistent with previous studies using unsanded membranes [14], while the wrinkle formation may be attributed to membrane shrinkage during drying or localized stress/strain from electrode particle growth. In contrast, the surface-roughened IPMCs (SD and FT; figures 2(c) and (e)) exhibited more pronounced topography, characterized by distinct peaks and valleys. This rough electrode surface can function as a porous layer facilitating water transport into and out of the membrane [12]. Also, the sanded samples showed the penetration of platinum electrodes into the membrane, as indicated by arrows in figure S2(b) and (d).

3.2. Surface resistance

The surface resistance of the IPMC electrodes also varied with the membrane pretreatment conditions. As shown in figure 3, IPMCs with surface roughening (SD and FT) exhibited lower electrical resistance compared to those fabricated without sanding (NP and CL). This contrasts with a prior study that rough surfaces typically increase resistance due to their porous structure and poor interfacial contact [12]. In present study, however, the lower surface resistance appears to correlate more closely with the greater electrode thickness and deeper penetration of electrode materials facilitated by sanding (figure S2) likely enhances electrical continuity, improving internal conductivity, even if the rough morphology leads to less ideal probe contact at the surface. Moreover, several studies have also shown that surface resistance decreases as electrode thickness increases [28, 29].

A comparison between the NP and CL samples further indicates that membrane cleaning significantly reduces surface resistance, even though it did not produce significant visual differences in surface morphology (figure 2, figure S1-2). This suggests that residual organic contaminants or surface impurities may disrupt electrode continuity or introduces barriers to electron transfer in the membrane-electrode interface. It should be noted that the IPMC sample with both sanding and cleaning FT showed not only the lowest surface resistance but also the smallest standard deviation, indicating a more uniform and consistent electrode structure across the sample.

3.3. Water uptake and dimensional changes of IPMC

The water uptake and dimensional changes of the IPMCs upon hydration were also influenced by the membrane surface pretreatment conditions. Water content is a critical parameter in IPMC actuation, as the electromechanical response is driven by the migration of water and cations under an applied electric field [12]. In addition, the degree of hydration affects the mechanical stiffness and electrical resistance of IPMCs [4]. As shown in table 2, IPMC samples with surface roughening (SD and FT) exhibited higher water uptake upon hydration compared to the CL sample. This higher water uptake in the sanded samples may be attributed to the porous electrode structures resulting from the rough surface morphology, which facilitates water entrapment within the electrode layer and at the electrode-membrane interface. Interestingly, the sample NP, which underwent neither sanding nor cleaning, also exhibited high water content, comparable to the SD and FT samples. One possible explanation for this is that surface residues or contaminants present on the untreated membrane NP may have altered the surface energy or pore structure in a way that promotes water retention.

Alternatively, the lower water uptake observed in the sample CL could be attributed to the prolonged exposure to hydrogen peroxide at a high temperature without surface roughening. This pretreatment condition may have partially

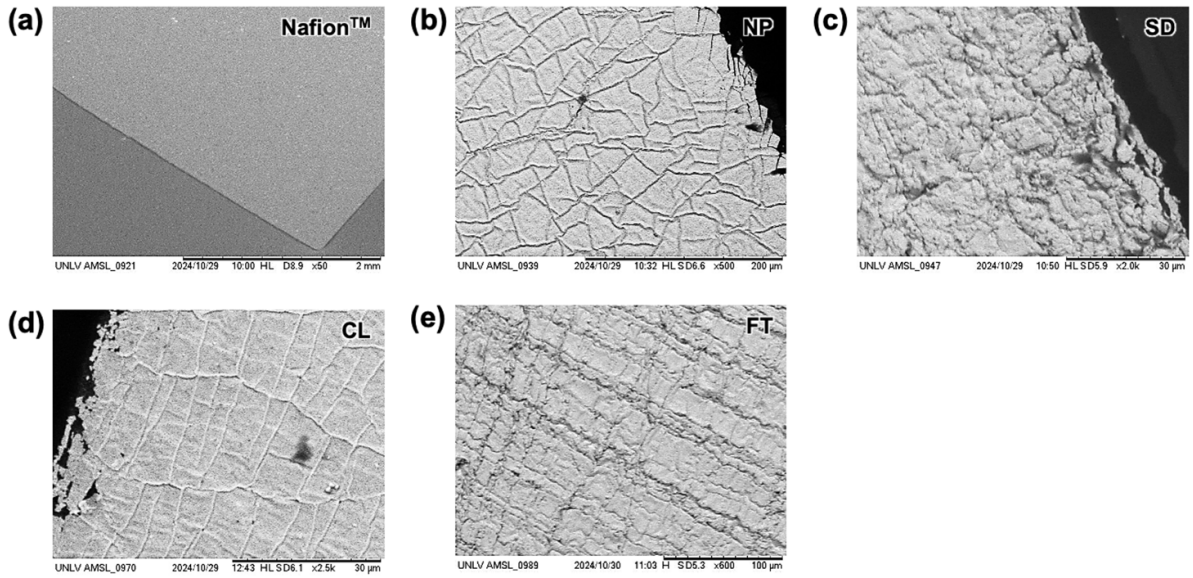

Figure 2. Surface morphology of IPMC electrodes fabricated with different membrane surface pretreatments. (a) Bare Nafion^{TM} 117 membrane as a reference. (b)–(e) IPMC surfaces fabricated with varying membrane surface treatments: (b) no pretreatment (NP), (c) sanding only (SD), (d) cleaning only (CL), and (e) fully treated (FT; sanding and cleaning).

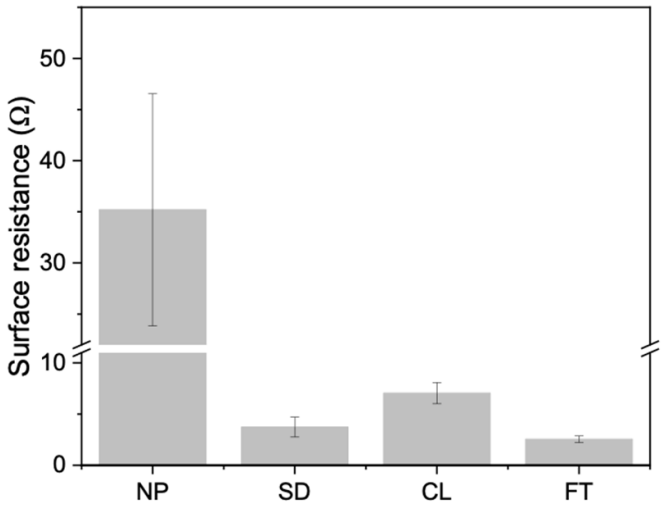

Figure 3. Surface resistance of IPMC films with different membrane surface pretreatments. Data are presented as mean ± standard deviation (N = 10).

Table 2. Water uptake and dimensional changes of IPMCs upon hydration, fabricated with different membrane surface pretreatment conditions. Data are presented as mean ± standard deviation (SD) from four independent specimens (N = 4), with more than five technical replicates per specimen.

	NP	SD	CL	FT
Water uptake (%)	14.1 ± 4.4	13.7 ± 3.8	6.8 ± 1.3	13.8 ± 2.1
Elongation rate (%)	8.8 ± 2.9	8.2 ± 3.9	5.1 ± 2	8.2 ± 0.9
Swelling (%)	9.3 ± 3	10.2 ± 2.6	6 ± 1.6	9.8 ± 2.3

degraded the sulfonic acid groups, which are responsible for water attraction, and potentially damaged the PTFE backbone, leading to a collapse of the porous structure and consequently lower water uptake. The dimensional expansion (elongate rate and thickness swelling) also followed the same trend as water uptake; samples with higher water uptake (NP, SD, and FT) exhibited greater dimensional changes upon hydration, while the CL sample showed lower expansion.

3.4. Actuation performance

To investigate the effects of the different membrane surface pretreatment conditions on IPMC actuation performance, tip displacement was recorded under a sinusoidal voltage, as shown in figure 4. The fully treated IPMC (FT), which underwent both sanding and sequential cleaning with hydrogen peroxide and sulfuric acid, exhibited significantly larger and more stable tip displacement than the partially treated samples (SD and CL) and sample NP. This notably better actuation performance of the FT sample correlates with its thicker electrodes and deeper penetration into the membrane (figure S2), lower surface resistance (figure 3), higher water uptake (table 2), and rough surface morphology (figure 1). It is known that a porous structure with membrane penetration promotes charge storage capacity and facilitates ion transport within IPMCs [12, 27]. Furthermore, low surface resistance contributes to a more uniform potential distribution, thereby improving the efficiency of cation and water migration and enhancing actuation performance [14]. Together, these factors lead to the enhanced and consistent bending response observed in the FT sample.

In contrast, the NP, SD, and CL samples exhibited lower actuation amplitudes and more irregular, noisy displacement waveforms. This diminished performance may result from a combination of factors, including poor electrode–membrane interface quality, limited porosity, thinner electrodes, and higher surface resistance, all of which hinder effective charge transfer and water migration. As reported by Wang *et al* [14], high surface resistance is associated with poor electrode continuity, leading to non-uniform potential distribution across the IPMC and consequently reducing actuation efficiency and stability. Interestingly, the actuation stability appeared to correlate with electrode thickness (figure S2) and surface roughness, underscoring the importance of achieving sufficient electrode deposition and sanding. Notably, although the CL sample exhibited a less stable and more irregular waveform than SD in the early phase of actuation, its larger overall tip displacement—and the fact that SD showed similarly weak and unstable actuation as NP—suggests that membrane cleaning is as important as surface roughening for achieving effective IPMC actuation.

3.5. SECM analysis

The IPMC samples were further analyzed using a SECM to evaluate the influence of membrane surface pretreatment conditions on local electrochemical activity and

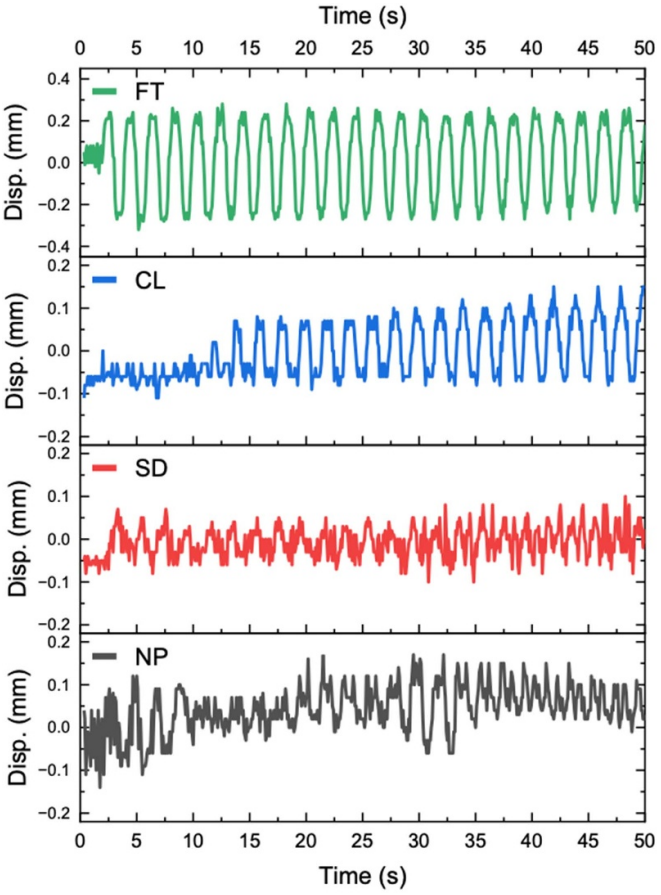

Figure 4. Representative tip displacement of IPMC strips, fabricated with different membrane surface pretreatment conditions under an applied sinusoidal voltage of ±1 V at 500 mHz. The voltage was applied at 2 s. Samples include no pretreatment (NP), sanding only (SD), cleaning only (CL), and fully treated (FT; sanding and cleaning).

electrode-membrane contrast. SECM enables spatially resolved electrochemical analysis, distinguishing between conductive platinum electrode regions and insulating membrane regions based on local redox activity [24, 30]. Prior to SECM imaging, CV was conducted in the bulk electrolyte solution, with the UME probe positioned far from the sample surface, to confirm steady-state, diffusion-limited redox behavior and to determine an appropriate tip bias. As shown in figure 5, the CV exhibits a characteristic diffusion-controlled, sigmoidal profile, with the current plateauing above approximately 0.55 V vs Ag/AgCl, indicating the onset of diffusion-limited regime. The redox reaction begins around 0.4 V, which is slightly higher than the standard electrode potential (0.32 V vs Ag/AgCl; 0.536 V vs SHE) [31], likely due to the dominance of the reduced form (I^-) over the oxidized form (I_3^-) in the electrolyte. Based on this result, a tip bias of 0.7 V vs Ag/AgCl was selected for SECM imaging to ensure stable operation within the diffusion-limited regime.

A flat model sample with a 5 mm gold disc mounted at the center was initially imaged to validate the SECM system.

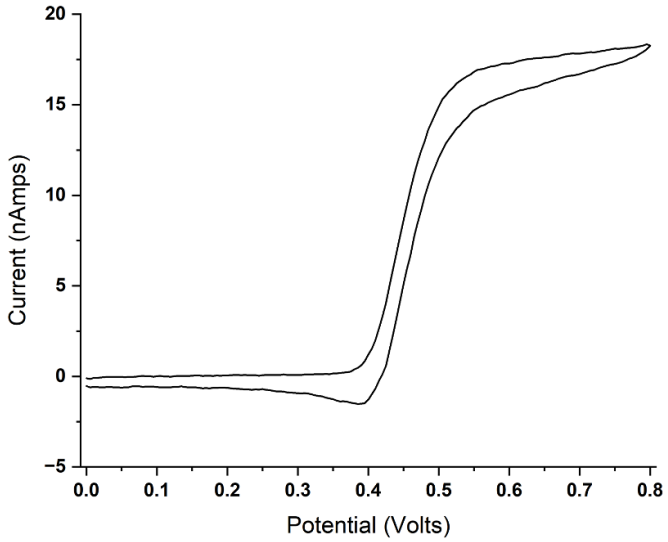

Figure 5. Cyclic voltammetry (CV) curve of the Pt ultramicroelectrode (UME) in bulk electrolyte solution (1 mM KI and 100 mM NaCl). The potential was scanned from 0 V to 0.8 V at a scan rate of 100 mV s^{-1}.

Figures 6(b) and (c) clearly distinguish the conductive circular gold substrate from the surrounding insulating epoxy region. In SECM mapping performed in feedback mode, the localized tip current changes based on the electrochemical activity of the substrate directly beneath the UME, allowing for the identification of conductive and insulating areas [24, 25, 32]. When the probe tip is positioned above the conductive gold electrode, the redox mediator undergoes electron transfer at the tip (e.g. $3I^- \rightarrow I_3^- + 2e^-$), and the complementary reaction occurs at the substrate surface. This regeneration of the mediator near the tip increases its flux back to the tip, resulting in enhanced tip current (positive feedback). In contrast, when the tip is above an insulating region such as an epoxy, the diffusion of the mediator is hindered and the regeneration is suppressed, leading to decreased tip current (negative feedback). As the gold disk and surrounding epoxy resin are flat, the distinct current contrast observed in figures 6(b) and (c) reflects this difference in electrochemical activity across the flat sample.

It should be noted that the tip current in SECM is also influenced by the absolute tip-substrate separation. Since the SECM imaging was conducted in constant-height mode, any surface height variations can alter the tip-surface distance, thereby affecting the diffusion of redox mediators to the tip and, consequently, the current signal. Therefore, surface topography can also appear as current gradients in SECM images, and the recorded SECM signal reflects a combination of both electrochemical activity of the substrate and its surface topography. In figure 6(c), the features observed over the gold substrate are likely due to microscale surface roughness, even though the surface appears visually smooth (figure 6(a)). However, the rough surface morphology seen in figure 2(e) does not appear in the SECM image (figure 6(e)) because the nanoscale peaks and valleys are smaller than the 25 μm-diameter UME tip and therefore cannot be resolved.

SECM imaging effectively distinguished the platinum electrode regions from the Nafion^{TM} membrane region in the cross-sectioned FT IPMC sample. As shown in figure 7, the 2D current map and 3D reconstruction (figures 7(b) and (c)) display two broad regions of elevated current, corresponding to the two platinum electrodes. Since Nafion is ionically conductive but electronically insulating, the region between the electrodes exhibits a lower current intensity than the platinum electrodes. The slightly sloped baseline observed in the line profile across the IPMC membrane (figure 7(d)) is due to a tilt in the resin substrate during mounting. The broad electrode peaks, wider than the actual electrode thickness observed in figure S2, are attributed to the relatively large UME tip diameter (10 μm) and/or to platinum nanoparticles that have penetrated into the membrane [14], which are not clearly visible in SEM images, compared to the main electrode layers. The non-flat, asymmetric profile within the membrane region, as well as the broader peak on the right side, likely reflects unequal electrode thicknesses, with the right-side electrode being thicker than the left, as seen in the SEM image (figure 7(a)). Minor current fluctuations along the line profile in figure 7(d) are likely due to surface roughness in the polished cross-section (figure 7(a)). Future work using a smaller UME tip diameter (e.g. 1 μm) is necessary for more detailed analysis.

Figure 8 presents SECM imaging of the cross-section of four different IPMC samples fabricated with different membrane surface pretreatments and embedded in UV resin. The 2D SECM map in figure 8(b) and the averaged current line profile in figure 8(c) clearly resolve the individual IPMC samples, with greater current contrast between the electrode regions and the membrane/UV resin region compared to figure 7. This enhanced resolution was achieved by positioning the UME probe very close to the surface (nearly in contact), resulting in near-zero current over the insulating resin. Although the 10 μm-diameter probe is larger than the electrode thickness, leading to broadened peaks in the line profile, the higher SECM current intensities observed in the SD and FT samples indicate more electrochemically active and continuous platinum electrode layers. This is consistent with their lower surface resistance (figure 3) as well as their larger electrode thickness and platinum penetration into the membrane observed in the cross-sectional SEM images (figure S2). This suggests that deeper and more integrated electrode formation enhances the local redox regeneration, resulting in stronger SECM signals. The higher SECM intensities may also reflect the greater actuation stability observed in these samples (figure 4). The anomalous current peak observed in the membrane region of the NP (at $X \approx 250$ μm) may be attributed to residual platinum particles left on the surface during cross-sectioning or inadvertently picked up by the probe during the near-surface scanning.

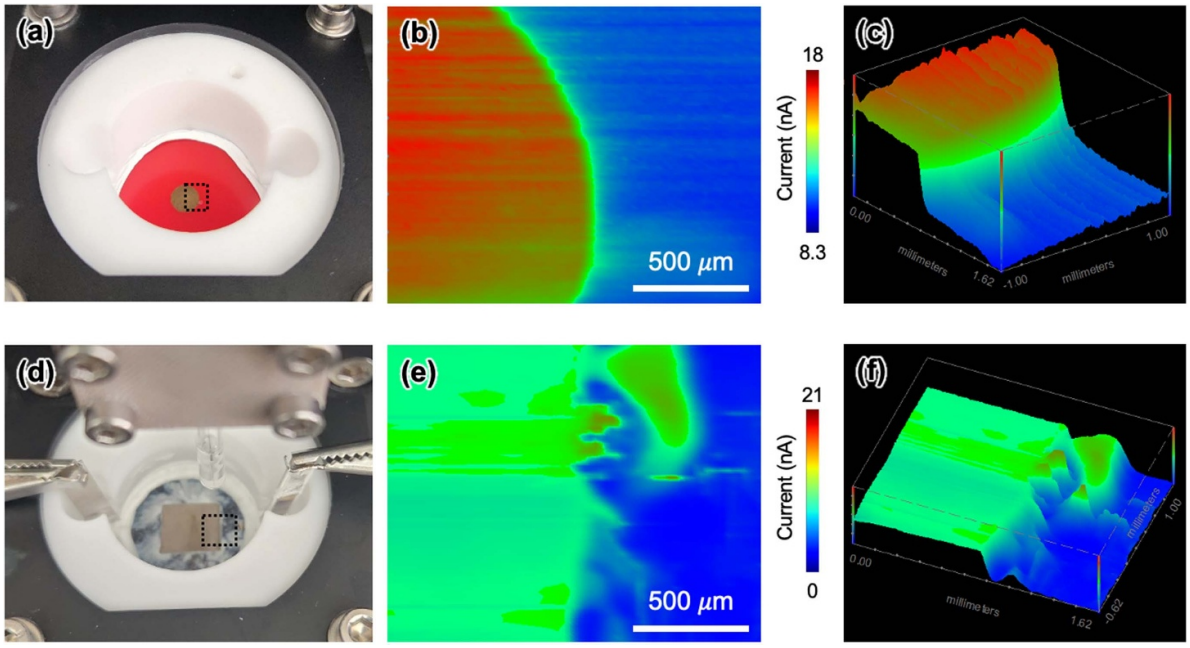

Figure 6. SECM imaging of a gold electrode and a fully treated IPMC (FT) surface using a 25 μm-diameter UME probe. (a), (d) Photographs of the gold electrode and IPMC embedded in epoxy, respectively; the dotted boxes indicate the scanned areas. (b), (e) Corresponding 2D SECM current maps showing contrast between the conductive (gold or platinum) and insulating (epoxy) regions. (c), (f) 3D reconstructions of SECM current intensity for the gold electrode (c) and IPMC surface (f).

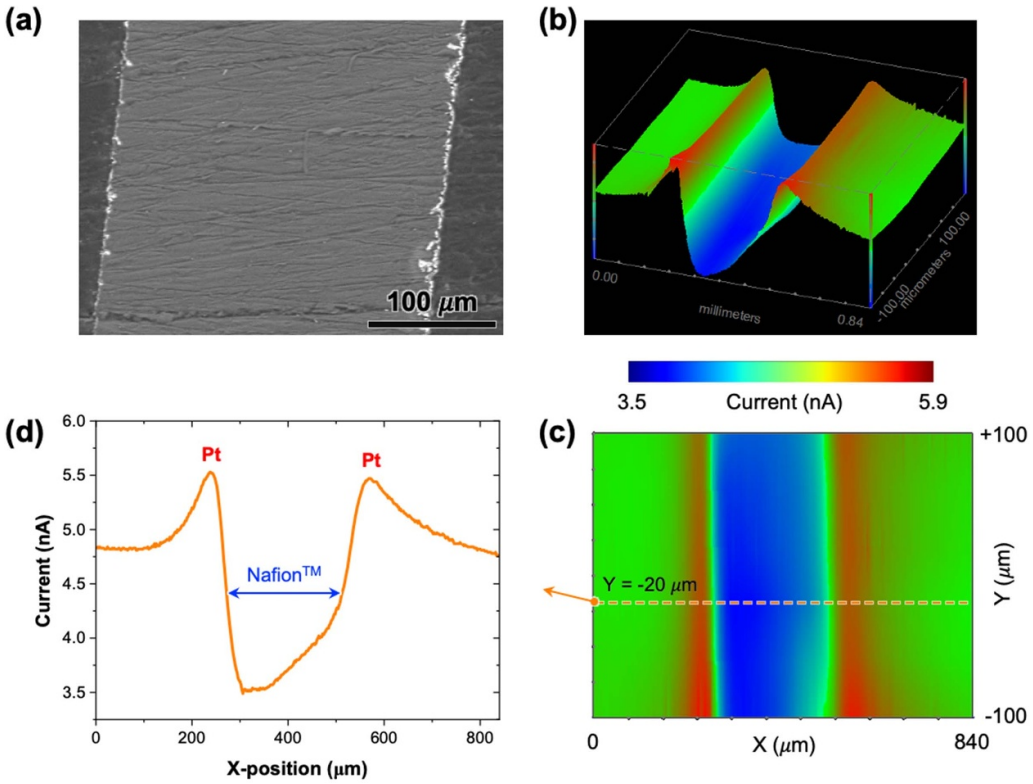

Figure 7. SECM imaging of a cross-sectioned fully treated (FT) IPMC sample, prepared by polishing, using a 10 μm-diameter UME probe. (a) SEM image of the FT IPMC sample embedded in UV-curable resin and polished to expose a cross-section. (b) 3D SECM current map of the scanned area (840 μm in the X-direction and 200 μm in the Y-directions, with step sizes of 2 μm and 40 μm, respectively). (c) Corresponding 2D SECM current map of the same region. (d) Current line profile along the dashed line ($Y = -20$ μm) in (c).

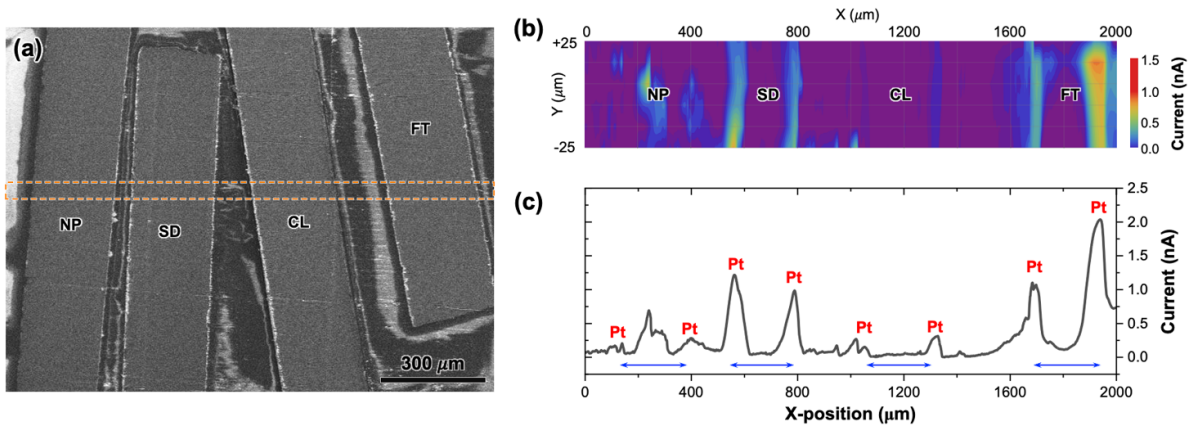

Figure 8. SECM imaging of cross-sectioned IPMCs embedded in a UV-curable resin, using a 10 μm-diameter UME probe. (a) SEM image of the cross-sectioned IPMC samples. The dashed orange box indicates the scanned area: 2000 μm (X-direction) $\times$ 50 μm (Y-direction), with step sizes of 2 μm (X) and 10 μm (Y). (b) 2D SECM current map of the scanned area. (c) Current line profile averaged over six horizontal line scans at Y = 0, 10, 20, 30, 40, and 50 μm. Blue double-sided arrows represent Nafion^{TM} membrane regions.

4. Conclusions

This study investigated how membrane surface pretreatment—specifically sanding and sequential cleaning with hydrogen peroxide and sulfuric acid—affects the physical and electrochemical properties of IPMCs and, in turn, their actuation performance. Surface roughening via sanding led to rougher electrode morphology, thicker electrode layers with platinum penetration into the membrane, lower surface resistance, stronger SECM signals, and more stable actuation, highlighting the importance of this step in promoting effective electrode formation. While surface cleaning alone reduced water uptake, it significantly lowered surface resistance and improved actuation compared to uncleaned samples, likely by removing impurities that hinder electrode continuity. The combination of sanding and cleaning yielded the most favorable results, with the fully treated IPMC showing the largest and most stable tip displacement, emphasizing the synergistic role of both treatments. Additionally, SECM analysis proved effective for visualizing the electrode and membrane layers in cross-sectioned IPMCs and characterizing local electrochemical activity that is not directly accessible via surface resistance measurements. Despite spatial resolution limitations due to thin electrode layers and the size of the UME tip, the strong redox contrast between platinum and Nafion enabled clear differentiation of structural regions. Overall, SECM serves as a powerful complementary tool for probing the electrochemical architecture of IPMCs, offering potential to investigate ion migration and interfacial charge dynamics within the membrane region, thereby advancing the fundamental understanding and development of high-performance, energy-efficient ionic polymer–metal composites.

Data availability statement

All data that support the findings of this study are included within the article (and any supplementary files).

Acknowledgments

This work was supported in part by the U.S. Department of Energy and the Savannah River National Laboratory under BSRA Contract 0000658475. We also acknowledge partial financial support from the Army Research Office under Award Number W911NF2310180.

Author contributions

Jung Hwa Lee
Data curation (equal), Formal analysis (equal), Investigation (lead), Methodology (equal), Software (equal), Validation (lead), Writing – original draft (lead), Writing – review & editing (equal)

Jongcheol Lee
Conceptualization (supporting), Data curation (equal), Formal analysis (equal), Investigation (equal), Methodology (equal), Validation (equal), Writing – original draft (supporting), Writing – review & editing (equal)

John Albert Faccinto 0009-0007-7820-5945
Data curation (supporting), Formal analysis (supporting), Methodology (supporting), Writing – review & editing (supporting)

Kwang J Kim 0000-0003-2134-4964
Conceptualization (lead), Formal analysis (supporting), Funding acquisition (lead), Investigation (equal), Methodology (supporting), Project administration (lead), Resources (lead), Software (lead), Supervision (lead), Validation (supporting), Visualization (supporting), Writing – review & editing (supporting)

References

[1] Hubbard J J, Fleming M, Palmre V, Pugal D, Kim K J and Leang K K 2014 Monolithic IPMC fins for propulsion and maneuvering in bioinspired underwater robotics *IEEE J. Oceanic Eng.* **39** 540–51

[2] Guo S, Ge Y, Li L and Liu S 2006 Underwater swimming micro robot using IPMC actuator *2006 Int. Conf. on Mechatronics and Automation* pp 249–54

[3] Chen Z, Bart-Smith H and Tan X 2015 IPMC-actuated robotic fish *Robot Fish: Bio-inspired Fishlike Underwater Robots* (Springer) pp 219–53

[4] Tang G, Mei D, Zhao X, Zhao C, Li L and Wang Y 2023 A comprehensive survey of ionic polymer metal composite transducers: preparation, performance optimization and applications *Soft. Sci.* **3** 9

[5] Brunetto P, Fortuna L, Giannone P, Graziani S and Pagano F 2010 A resonant vibrating tactile probe for biomedical applications based on IPMC *IEEE Trans. Instrum. Meas.* **59** 1453–62

[6] McDaid A J, Xie S Q and Aw K C 2012 A compliant surgical robotic instrument with integrated IPMC sensing and actuation *Int. J. Smart. Nano. Mater.* **3** 188–203

[7] Napollion L and Kim K J 2024 Ionic polymer-metal composite (IPMC) as a flexible capacitor: an experimental study *Smart Mater. Struct.* **33** 125009

[8] Nagel W S, Fakharian O, Aureli M and Leang K K 2024 Engineered IPMC sensors: modeling, characterization, and application towards wearable postural-tactile measurement *Smart Mater. Struct.* **33** 015035

[9] Ostretsov K I, Orekhov Y D, Khmelnitskiy I K, Aivazyan V M, Testov O A, Gareev K G, Testov D O, Karelin A M and Bagrets V S 2021 Heart rate monitor based on IPMC sensor *2021 Int. Conf. on Electrical Engineering and Photonics (Eexpolytech)* pp 139–42

[10] Tiwari R and Garcia E 2011 The state of understanding of ionic polymer metal composite architecture: a review *Smart Mater. Struct.* **20** 083001

[11] Tiwari R and Kim K J 2013 IPMC as a mechanoelectric energy harvester: tailored properties *Smart Mater. Struct.* **22** 015017

[12] Shahinpoor M and Kim K J 2001 Ionic polymer-metal composites: i. Fundamentals *Smart Mater. Struct.* **10** 819

[13] Chang L, Chen H, Zhu Z and Li B 2012 Manufacturing process and electrode properties of palladium-electroded ionic polymer–metal composite *Smart Mater. Struct.* **21** 065018

[14] Wang Y, Zhu Z, Chen H, Luo B, Chang L, Wang Y and Li D 2014 Effects of preparation steps on the physical parameters and electromechanical properties of IPMC actuators *Smart Mater. Struct.* **23** 125015

[15] Wang J, Wang Y, Zhu Z, Wang J, He Q and Luo M 2019 The effects of dimensions on the deformation sensing performance of ionic polymer-metal composites *Sensors* **19** 2104

[16] Wang Y, Tang G, Zhao C, Wang K, Wang J, Ru J, Sheng J, Chang L and Li L 2021 Experimental investigation on the physical parameters of ionic polymer metal composites sensors for humidity perception *Sens. Actuators B* **345** 130421

[17] Wang Y, Chen H, Wang Y, Zhu Z and Li D 2014 Effect of dehydration on the mechanical and physicochemical properties of gold- and palladium -ionomeric polymer-metal composite (IPMC) actuators *Electrochim. Acta* **129** 450–8

[18] Kim K and Shahinpoor M 1999 Effect of the surface-electrode resistance on the actuation of ionic polymer-metal composite (IPMC) artificial muscles *Proc. SPIE* 3669 308–19

[19] Shahinpoor M and Kim K J 2002 Experimental study of ionic polymer-metal composites in various cation forms: actuation behavior *Sci. Eng. Compos. Mater.* **10** 423–36

[20] Biswal D K, Bandopadhya D and Dwivedy S K 2013 Investigation and evaluation of effect of dehydration on vibration characteristics of silver-electroded ionic polymer–metal composite actuator *J. Intell. Mater. Syst. Struct.* **24** 1197–212

[21] Kim D and Kim K J 2006 Experimental investigation on electrochemical properties of ionic polymer–metal composite *J. Intell. Mater. Syst. Struct.* **17** 449–54

[22] Napollion L and Kim K J 2023 Electrochemical performance of ionic polymer metal composite under tensile loading *Smart Mater. Struct.* **32** 095025

[23] Tiwari R and Kim K 2008 Improved IPMC sensing by use of cation and through induced nano-to-micro scale surface cracks *Proc. SPIE* 6932 1057–68

[24] Zhang X, Han C and Xu W 2023 Imaging analysis of scanning electrochemical microscopy in energy catalysis *Chem. Biomed. Imaging* **1** 205–19

[25] Bard A J, Fan F-R F, Pierce D T, Unwin P R, Wipf D O and Zhou F 1991 Chemical imaging of surfaces with the scanning electrochemical microscope *Science* **254** 68–74

[26] Szunerits S, Pust S E and Wittstock G 2007 Multidimensional electrochemical imaging in materials science *Anal. Bioanal. Chem.* **389** 1103–20

[27] Kwang J K and Mohsen S 2003 Ionic polymer–metal composites: II. Manufacturing techniques *Smart Mater. Struct.* **12** 65

[28] Onishi K, Sewa S, Asaka K, Fujiwara N and Oguro K 2001 Morphology of electrodes and bending response of the polymer electrolyte actuator *Electrochim. Acta* **46** 737–43

[29] Kim S J, Kim S-M, Kim K J and Kim Y H 2007 An electrode model for ionic polymer–metal composites *Smart Mater. Struct.* **16** 2286

[30] Shi X, Qing W, Marhaba T and Zhang W 2020 Atomic force microscopy—Scanning electrochemical microscopy (AFM-SECM) for nanoscale topographical and electrochemical characterization: principles, applications and perspectives *Electrochim. Acta* **332** 135472

[31] Bard A J F and Larry R 2001 *Electrochemical Methods: Fundamentals and Applications* 2nd edn (Wiley)

[32] Bard A J, Fan F R F, Kwak J and Lev O 1989 Scanning electrochemical microscopy. Introduction and principles *Anal. Chem.* **61** 132–8